JOURNAL OF MATERIALS SCIENCE 25 (1990) 2367–2378

Tensile behaviour of blends of poly(vinylidene fluoride) with poly(methyl methacrylate)

PEGGY CEBE*, SHIRLEY Y. CHUNG
Applied Sciences and Microgravity Experiments Section, Jet Propulsion Laboratory, California Institute of Technology, Pasadena, California 91109, USA

Blends of poly(vinylidene fluoride) (PVF_2) and poly(methyl methacrylate) (PMMA) were prepared over a wide concentration range and tested in tension at the same relative temperature below the glass transition. Testing was performed at strain rates ranging from 10 to 0.01 min^{-1} at test temperatures from T_g-40 to T_g-10. By normalizing the test temperature to fixed increments below T_g, blends and homopolymers can be compared on the basis of PVF_2 and PMMA composition and crystallinity. In nearly all blends, under conditions favouring disentanglement, (decrease in strain rate, or increase in test temperature), the yield stress and drawing stress decreased while the breaking strain increased. For materials with about the same degree of crystallinity, those with a higher proportion of amorphous PVF_2 exhibited brittle-like behaviour as a result of interlamellar tie molecules. In the semicrystalline blends, yield stress remains high as the test temperature approaches T_g, whereas in the amorphous blends the yield stress falls to zero near T_g. Results of physical ageing support the role of interlamellar ties which cause semicrystalline blends to exhibit ageing at temperatures above T_g.

1. Introduction

Poly(vinylidene fluoride) (PVF_2) and poly(methyl methacrylate) (PMMA) can be blended in the melt to form one of the few miscible blend systems [1]. PVF_2/PMMA blends have been studied extensively using a variety of techniques to determine miscibility [1–10]. At elevated temperatures, a liquid–liquid phase separation occurs [11, 12], and at temperatures below the melting point, PVF_2 can crystallize [13–21] into what was at first thought to be strictly a two-phase system. However, an upper critical solution temperature has been reported for annealed blends [22, 23]. Recent work [24, 25] provides strong evidence for the existence of three distinct regions: purely crystalline PVF_2, purely amorphous PVF_2 located at the crystal–amorphous interface, and a mixed region of amorphous PVF_2 and PMMA. A variety of bulk property measurements has been reported on PVF_2/PMMA blends. Properties such as sorption kinetics [26], rheological behaviour [27], piezoelectric [28] and dielectric response [24, 25, 28–31], and optical birefringence [32] have been studied to determine whether blending results in enhancement of specific characteristics.

Mechanical properties have been reported for the elucidation of relaxation phenomena [3, 4, 22, 33], effects of orientation on structure [30, 34], and composition dependence of tensile properties [1, 35, 36]. The present work reports results of tensile property measurements, designed to study the effects of strain rate, test temperature and composition ratio. Previous investigations of the tensile properties involved testing all blends at the same temperature regardless of the location of the glass transition relative to the test temperature [35, 36]. Thus, effects of blend composition could not be separated from the testing conditions in which some blends were tested above T_g while others were tested below T_g [35, 36]. We have undertaken a study of the tensile behaviour of PVF_2/PMMA blends over a wide range of test conditions designed to probe the temperature and strain-rate dependence of the stress–strain behaviour. We have utilized a testing situation in which the test temperature is normalized with respect to the glass transition of each blend. In this way, effects of absolute test temperature have been minimized. All blends have been tested in the glassy state.

2. Experimental details

PVF_2 was obtained from Pennwalt Corp., Philadelphia, PA, under the brand name Kynar (RC-9816-21). No other information was available about this polymer. PMMA was obtained from Polysciences, Warrington, PA, and had an intrinsic viscosity of 1.4. Molecular weights determined by gel permeation chromatography (GPC) in methylene chloride were M_n = 190 000 and M_w = 415 000, using a polystyrene standard.

Blends were obtained by the following procedure. PVF_2 was dissolved at room temperature in dimethylacetamide (DMA). Under argon gas flow, the solution was gently heated to about 110°C with continuous

* *Present address:* Department of Materials Science and Engineering, Massachusetts Institute of Technology, 13-5082 Cambridge, Massachusetts 02139, USA.

0022–2461/90 $03.00 + .12

stirring. The PMMA was added to this solution, and dissolved completely after a few hours. The cooled blend solution was slowly precipitated into a large volume of methanol (about ten times the DMA volume) with constant stirring. The precipitate was partially dried, chopped to a coarse mix, then dried at ambient conditions for 2 wk. The coarse powder was further dried under vacuum at 60° C for several days.

Mechanical test films were prepared by compression moulding the blend powder at 190° C between ferrotype plates. The films were quenched into water and dried completely before being cut into straight-sided tensile specimens. Prior to testing, all blends were subjected to the same thermal history to eliminate effects of long storage at room temperature. The test strips were heated to 115° C for several minutes, then cooled rapidly to room temperature and tested immediately.

Thin films (7.62 cm × 0.635 cm × 0.0178 cm) were drawn in tension in an Instron tensile tester equipped with an environmental chamber. Nominal strain rates were 0.01, 0.1, 1.0 and 10 min^{-1} calculated from the fixed cross-head speed. True stress was calculated from engineering stress by using the cross-sectional area determined from the nominal strain (determined from cross-head displacement).

Samples were characterized before testing using differential scanning calorimetry (DSC) to determine melting point and degree of crystallinity in the semicrystalline blends. The heat of fusion of PVF_2 was assumed to be 104.2 J g^{-1} [37] for completely crystalline material. Wide-angle X-ray scattering (WAXS) was used to determine degree of crystallinity and relative degree of crystal perfection. The glass transition temperature was determined using thermomechanical analysis (TMA), DSC, and volume dilatometry, though not all techniques were used on all the blends.

3. Results

3.1. Material characterization

In Table I, the as-prepared blends are listed according to weight ratio of the starting materials, and this designation is used throughout. The measured glass transition temperature and degree of crystallinity are listed in columns two and three. The amount of amorphous PVF_2 (a-PVF_2) can be determined from the degree of crystallinity. Weight fraction a-PVF_2 is listed in column 4 of Table I, and is used to calculate a ratio of a-PVF_2 to PMMA, shown in the last column of Table I, normalized to 100%. For the present we make no distinction about whether the amorphous PVF_2 is located in an interphase region, or whether it is mixed with the PMMA. This point will be discussed in Section 4.

From Table I we see that the degree of crystallinity changes only 5% as the blend composition ratio changes from 75/25 to 100/0. The main effect of addition of 10% to 25% PMMA to pure PVF_2 is to change the nature of the amorphous regions, making them rich in PMMA. Addition of 40% to 60% PMMA results in marked decrease in the degree of crystallinity. Two blends, 60/40 and 40/60, have about the same ratio of a-PVF_2 to PMMA, although 60/40 has a degree of crystallinity of 37% whereas 40/60 is completely amorphous. In the semicrystalline blends, the crystals serve to broaden the glass transition region, and increase T_g compared to its value in an amorphous blend of the same composition.

DSC scans were obtained on the as-quenched materials and are shown in Fig. 1a. Scans were taken from 40 to 220° C at a scanning rate of 20° C min^{-1}. All samples exhibit a small endothermic response in the vicinity of 80° C as reported in earlier works [26, 29]. The feature is most pronounced in the 40/60 and 60/40 blends. In addition to the low-temperature endothermic response, all semicrystalline materials show a higher temperature endotherm whose position shifts upwards in temperature as the PVF_2 content increases, an effect that has been noted before [3, 15, 19]. No evidence of beta (form I) or gamma (form III) phase PVF_2 crystals was detected from the high-temperature endotherm, which appears to be due solely to melting alpha (form II) phase PVF_2 crystals [38, 39].

Previously we have seen evidence that the amorphous blends showed an "ageing" peak when stored below their glass transitions. We heated each material to 115° C and immediately cooled it to room temperature and rescanned. The results of the second scans are shown in Fig. 1b. The endotherm near 80° C is now completely absent in the amorphous materials 0/100, 10/90 and 40/60, and the glass transition can clearly be seen. In these samples the low-temperature endotherm is an artefact, and is related to the length of time the samples are held at room temperature before scanning, as well as to the rate of quenching through the glass transition. If the original cooling rate is less than the subsequent heating rate, an endothermic peak develops near the glass transition [40].

In the second scans of the semicrystalline blends, the small endotherm has been shifted to a temperature above 115° C (approximately to 130° C) indicating that the low-temperature endotherm in these materials is an annealing peak, due to the melting of a small

TABLE I Glass transition, crystallinity and amorphous PVF_2 fraction in PVF_2/PMMA blends

PVF_2/PMMA, (g/g)	T_g (° C)	Crystalline weight fraction	a-PVF_2 weight fraction	a-PVF_2/PMMA (g/g)
0/100	85	0.0	0.0	0/100
10/90	75	0.0	0.10	10/90
40/60	45	0.0	0.40	40/60
60/40	53	0.37	0.23	37/63
75/25	35	0.42	0.33	57/43
90/10	−8	0.44	0.46	82/18
100/0	−40	0.47	0.53	100/0

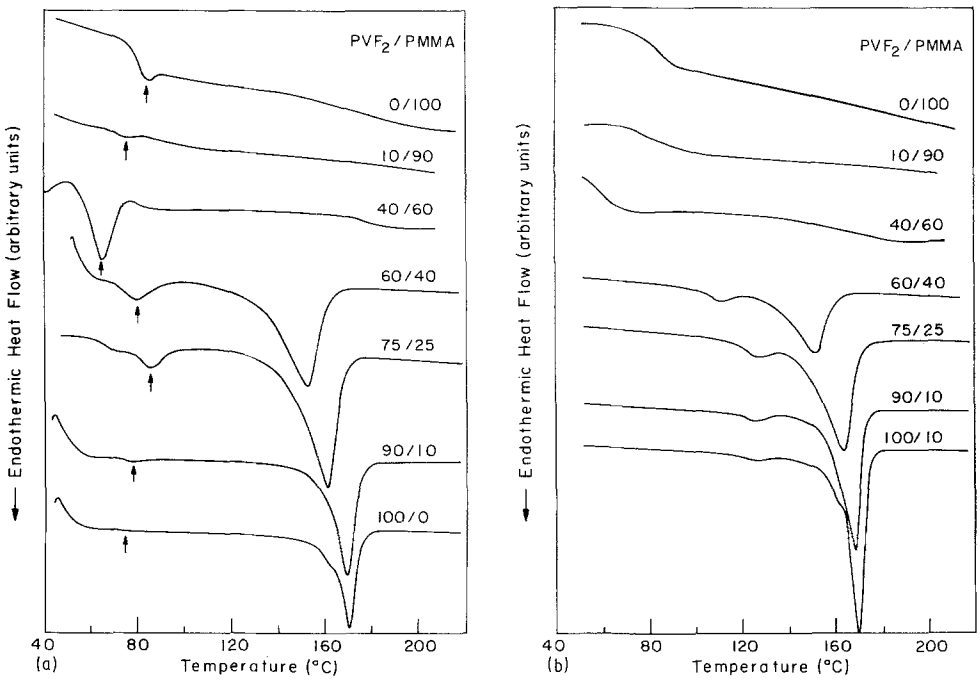

Figure 1 Endothermic response of PVF_2/PMMA blends (a) immediately after quenching from 190° C to room temperature and (b) immediately after heat treatment at 115° C followed by quenching to room temperature. $\dot{T} = 20°\,C\,min^{-1}$. See text for explanation of arrows indicating secondary endotherms.

population of imperfect crystals which had formed during cooling. This population has been perfected by the heat treatment and now melts at a higher temperature.

Wide-angle X-ray scattering curves are shown in Fig. 2 for the homopolymers and several blends. The scans were taken immediately after the materials were heat treated at 115° C, and thus are representative of the physical state just prior to tensile testing. Blend 10/90 was omitted for clarity. Pure PMMA exhibits two very broad amorphous scattering peaks centred at 14° and 30°. The main result of the addition of 40 wt % PVF_2 in the amorphous 40/60 blend is a shift in the centre of the amorphous scattering peak from 14° to 17°. The amorphous PMMA peak diminishes in relative intensity with increasing PVF_2 content in the 60/40, 75/25, and 90/10 materials. The crystalline reflections sharpen as perfection improves with increasing PVF_2 content. All reflections can be indexed to non-polar alpha phase or to polar gamma phase [39, 41, 42]. No reflections from the polar beta phase were observed [43].

Using Fourier transform-infrared spectroscopy (FTIR), two groups report composition-dependent changes in intensity of certain absorption bands in melt-quenched blends [18, 25, 44]. Hahn *et al.* [25] identify alpha phase from absorption bands at 531 and 410 cm^{-1}, and beta phase from 508 and 441 cm^{-1}. In their report Hahn *et al.* quote Kobayashi *et al.* [45] for beta at 441 cm^{-1}, which disagrees slightly with the beta band assignment of Bachmann *et al.* [46] and Hasegawa *et al.* [47]. More important is that the polar gamma phase also has absorption bands at 510 and 440 cm^{-1} [45–47]; thus absorption at these frequencies is not a clear indicator of beta-phase crystals. Details of sample preparation were not given by Hahn *et al.* [25]. However, Grubb and co-workers [48, 49] have shown that the presence of ionic impurities causes gamma phase to form preferentially over beta under conditions typically used for infrared analysis. These typical preparations include those used by Leonard *et al.* [18, 44], namely casting films from DMA

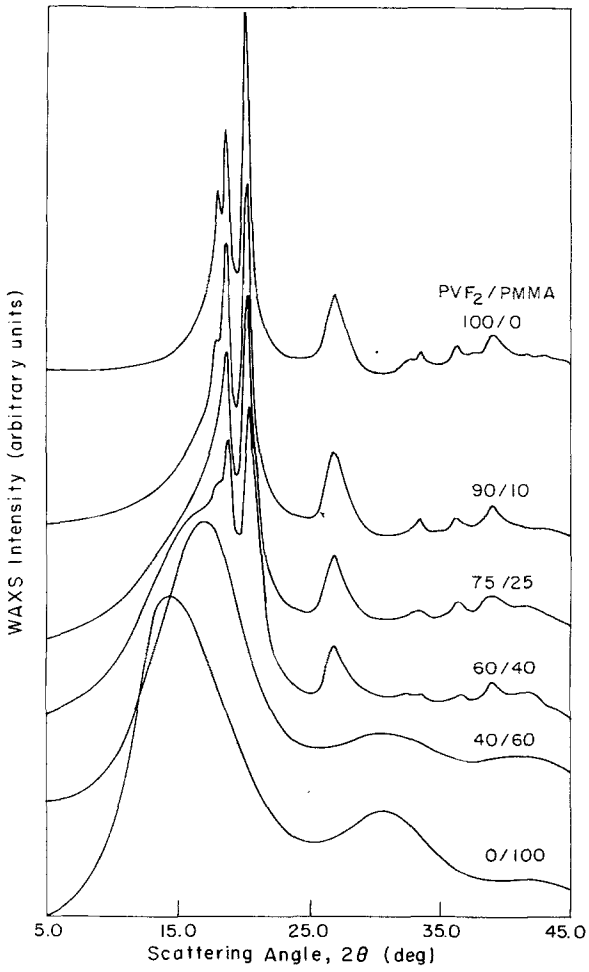

Figure 2 Wide-angle X-ray scattering intensity plotted against scattering angle for blends after heat treatment at 115° C. Blend 10/90 is omitted for clarity.

solutions onto salt discs. We have shown that only very small quantities of ionic impurities are needed to stimulate formation of gamma-phase crystals [49], therefore we regard this sample preparation as unsuitable for the purposes of FTIR phase identification. We consider the issue of beta-phase formation to be unresolved at this point. For the samples used in the present study, we see no unambiguous evidence for the existence of beta-phase crystals, all beta-phase absorption bands overlapping either with gamma-phase PVF_2 or with PMMA absorption bands.

3.2. Stress–strain behaviour: effects of test temperature

Five blends were tested in tension at four normalized test temperatures and four strain rates. Because of the very large number of stress–strain curves obtained under sixteen test conditions, we show only a selected subset of the data. Representative examples of engineering stress are plotted against nominal strain at a fixed strain rate for the homopolymers and blends in Figs 3 to 8. The figures depict the variation in tensile behaviour at fixed strain rate as the test temperature varies from T_g-40 to T_g-10. In most cases the fastest strain rate of $10.0\,min^{-1}$ is shown. Yield stress, fracture stress, and strain at break are summarized in Tables II to IV, respectively. In Table II the engineering yield stress is listed for those blends exhibiting strain softening; otherwise the extrinsic yield appears in Table II (see [50]).

Pure PVF_2 (100/0), shown on the left side of Fig. 3, was brittle at all test temperatures and strain rates. Test temperature did not affect the fracture stress in a regular manner for 100/0. Because of the brittle-like behaviour, only a limited number of tests were performed on this material. The lowest test temperature (T_g-40) and fastest strain rate ($10.0\,min^{-1}$) were not tested for PVF_2 homopolymer.

Addition of 10 wt % PMMA to PVF_2 results in the tensile testing behaviour shown for 90/10 on the right side of Fig. 3. Stress level and modulus decrease in 90/10 compared to 100/0. Irregular behaviour was seen in 90/10 as a function of test temperature. The behaviour shown in Fig. 3 indicates that 90/10 may be yielding at the higher test temperatures. However, as a result of the very low absolute temperature used for testing of 90/10, frost on the door of the environmental chamber prevented us from observing the blend during drawing. Thus, we are unable to say whether the decrease in stress observed in 90/10 might be the result of formation of a tear rather than the result of strain softening. Fracture properties of 90/10 failed to show any clear trends with strain rate or test temperature. Only at a slower strain rate of $0.1\,min^{-1}$

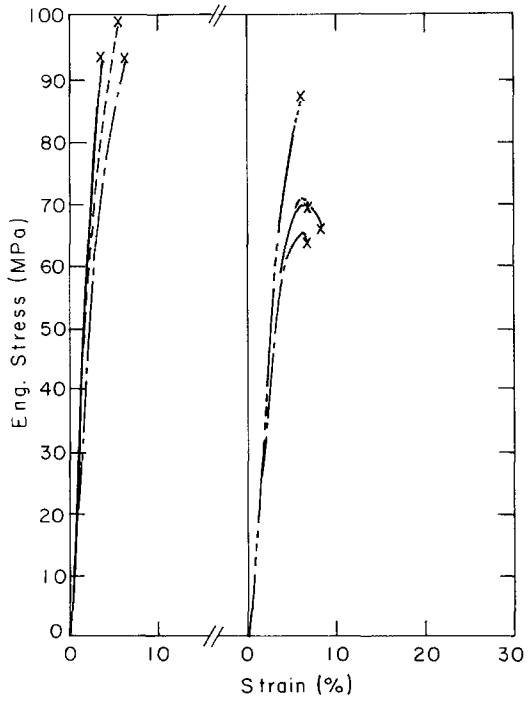

Figure 3 Engineering stress–strain curves for PVF_2 homopolymer (left) and blend 90/10 (right) at $\dot{\varepsilon} = 1.0\,min^{-1}$ and (----) T_g-40, (——) T_g-30, (– – –) T_g-20, (– – –) T_g-10.

TABLE II Engineering yield stress for PVF_2/PMMA blends

Test temp. (°C)	Strain rate (min^{-1})	σ_y (MPa) for Compositions PVF_2/PMMA:						
		0/100	10/90	40/60	60/40	75/25	90/10	100/0
T_g – 40	10.0	×	×	×	×	77	×	–
	1.0	54	57	61	59	74	×	–
	0.1	44	45	47	49	65	×	–
	0.01	39	39	39	41	58	72	–
T_g – 30	10.0	×	×	58	54	67	×	–
	1.0	33	51	47	48	63	70	×
	0.1	27	40	40	38	54	73	–
	0.01	17	27	29	29	49	70	×
T_g – 20	10.0	34	50	49	48	60	71	–
	1.0	25	43	36	40	52	71	×
	0.1	17	30	24	28	47	70	–
	0.01	10	16	15	23	40	75	×
T_g – 10	10.0	24	43	36	39	54	×	–
	1.0	18	36	26	29	46	65	×
	0.1	9	23	18	23	39	66	×
	0.01	7	16	8	16	33	×	×

× The sample fractured before yielding.
–The sample was not tested under these conditions.

TABLE III Engineering fracture stress for PVF_2/PMMA blends

Test temp. (°C)	Strain rate (min^{-1})	σ_b (MPa) for Compositions PVF_2/PMMA:						
		0/100	10/90	40/60	60/40	75/25	90/10	100/0
T_g − 40	10.0	49	66	72	63	76	84	–
	1.0	47	53	42	53	74	87	–
	0.1	41	39	43	37	56	83	–
	0.01	33	28	31	(41)	55	70	–
T_g − 30	10.0	46	58	53	31	65	86	–
	1.0	22	43	33	33	60	66	93
	0.1	21	30	27	(38)	48	73	–
	0.01	14	19	(29)	(29)	46	70	89
T_g − 20	10.0	20	33	30	26	59	70	–
	1.0	15	30	25	27	50	70	99
	0.1	13	(30)	(24)	(28)	42	67	–
	0.01	9	14	(15)	(23)	37	74	84
T_g − 10	10.0	14	28	23	22	50	72	–
	1.0	12	25	(26)	20	36	64	93
	0.1	(07)	17	13	(23)	37	65	85
	0.01	5	14	(08)	(16)	14	75	73

– The sample was not tested under these conditions.
( ) The test was halted before fracture occurred.

did the stress–strain curves exhibit any regularity, the fracture stress increasing as the test temperature decreased.

Effects of the addition of 25 wt % PMMA are shown in Fig. 4 for 75/25. As the temperature increases toward T_g, the drawing stress decreases, fracture stress decreases, and strain-to-break increases. The degree of crystallinity in 75/25 has been reduced only slightly, to 42% compared to 44% crystallinity in the 90/10 blend. Tensile properties, on the other hand, changed dramatically. Yield behaviour was observed at almost all strain rates and test temperatures. From data in Table II we see that clear trends exist in the yield behaviour of 75/25. At each test temperature the yield stress decreases as strain rate decreases; at a given strain rate, yield stress decreases as test temperature increases towards the glass transition. The stress–strain curves were quite broad near yield, and stress generally decreased steadily until failure. In a few cases (T_g-10 at 1.0 min^{-1}, T_g-20 and T_g-30 at 0.1 min^{-1}) necking occurred. The fracture properties of 75/25 indicate that breaking stress decreases with decreasing strain rate or increasing test temperature. Breaking strain generally increased with decreasing strain rate or increasing temperature, and in cases where this trend was not followed, premature failure at a flaw is the likely cause.

Tensile behaviour of 60/40 blend is shown in Fig. 5. Compared to 75/25, this blend can be drawn to very high strain levels before failure. At T_g-40, 60/40 is brittle, but large plastic deformation occurs as the test temperature increases towards T_g. The deformation beyond yield appears to be homogeneous as no necking was observed. At the highest strain no strain hardening was observed in this material.

The two amorphous blends, 40/60 and 10/90, are

TABLE IV Breaking strain for PVF_2/PMMA blends

Test temp. (°C)	Strain rate (min^{-1})	ε_b (%) for Compositions PVF_2/PMMA:						
		0/100	10/90	40/60	60/40	75/25	90/10	100/0
T_g − 40	10.0	11	6	7	5	9	6	–
	1.0	11	7	17	14	10	6	–
	0.1	10	13	10	42	18	6	–
	0.01	13	43	17	(36)	18	7	–
T_g − 30	10.0	6	6	11	31	9	8	–
	1.0	57	12	15	25	9	8	4
	0.1	60	23	11	(39)	16	7	–
	0.01	25	49	(45)	(79)	15	8	5
T_g − 20	10.0	39	23	25	63	11	8	–
	1.0	18	27	73	94	11	7	6
	0.1	52	(66)	(77)	(98)	24	9	–
	0.01	75	71	(17)	(78)	26	8	6
T_g − 10	10.0	74	25	148	82	15	8	–
	1.0	52	36	(96)	94	21	7	7
	0.1	(98)	57	68	(99)	22	7	7
	0.01	95	38	(99)	(100)	14	10	6

– The sample was not tested under these conditions.
( ) The test was halted before fracture occurred.

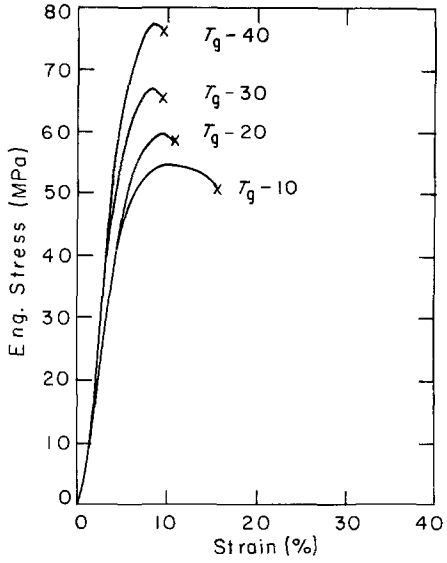

Figure 4 Engineering stress–strain curves for blend 75/25 at $\dot{\varepsilon} = 10.0\,\text{min}^{-1}$ and the temperatures indicated.

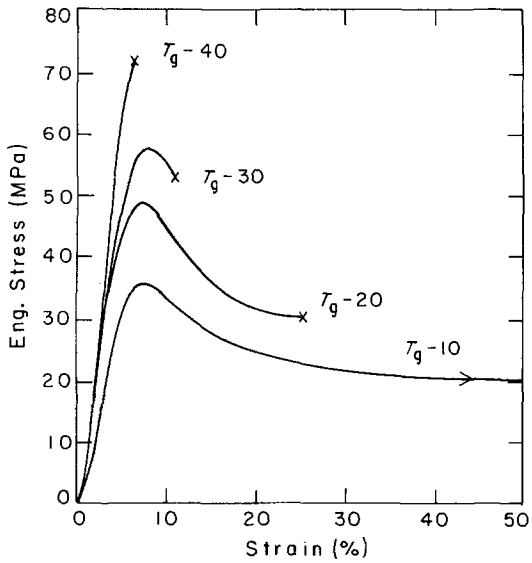

Figure 6 Engineering stress–strain curves for blend 40/60 at $\dot{\varepsilon} = 10.0\,\text{min}^{-1}$ and the temperatures indicated.

shown in Figs 6 and 7, respectively. Tensile behaviour of 40/60 is generally very similar to 60/40 (Fig. 5). At the lowest temperature, brittle failure is observed. Drawing stress decreases, and strain-to-break increases, as test temperature approaches T_g. At T_g-10, blend 40/60 draws to 148% strain at a nearly constant level of stress. No strain hardening was observed under any condition in 40/60.

In Fig. 7, tensile behaviour of blend 10/90 is shown. The general trends seen in the other blends are followed here as well, with fracture stress decreasing and strain-to-break increasing from T_g-40 to T_g-10. In comparison to 40/60, blend 10/90 appears to be more brittle. The breaking strain is reduced at all test temperatures, and yield stress is greater in 10/90 than in 40/60 when the same relative temperature is compared.

Pure PMMA (0/100) tensile behaviour is shown in Fig. 8. The material exhibits brittle-like behaviour at T_g-30. As the test temperature increases, 0/100 draws to much large strain-to-break, well over 70% at T_g-10. The drawing stresses are smaller than either 10/90 or 40/60 when the same relative temperatures are compared.

In Figs 9a, b and 10a, b the tensile behaviour is shown in a manner facilitating direct comparison of the different materials. Fig. 9 shows the tensile properties at a strain rate of $1.0\,\text{min}^{-1}$ for test temperatures of T_g-30 (Fig. 9a) and T_g-20 (Fig. 9b). In Fig. 9a, fracture stress and modulus decrease in the sequence 100/0 > 90/10 > 75/25 > 60/40 > 40/60. Then there is a jump at 10/90 to higher yield stress, modulus, and fracture stress. The pure PMMA 0/100 material exhibits brittle-like behaviour at T_g-30, fracturing before yield at a stress level lower than the yield stress of 10/90. In Fig. 9b, significantly greater amount of plastic deformation takes place when, for the same strain rate, the test temperature increases to T_g-20. Once again the fracture stress and modulus decrease, and strain-to-break is seen to increase from 100/0 to 40/60. Stress level increases at 10/90, then falls again at 0/100, similar to the behaviour seen in Fig. 9a. At T_g-20, pure PMMA 0/100 now yields and draws at

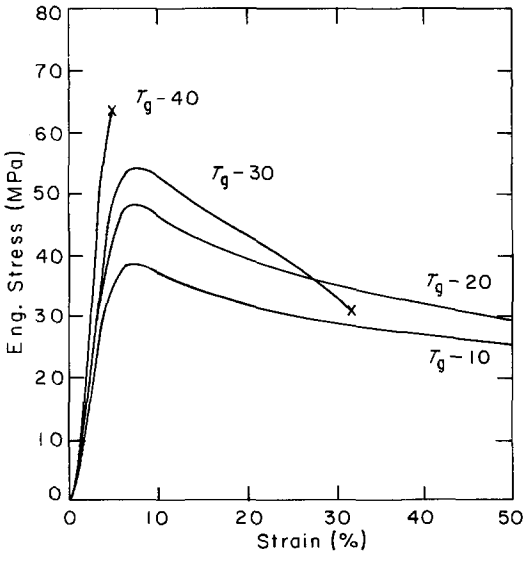

Figure 5 Engineering stress–strain curves for blend 60/40 at $\dot{\varepsilon} = 10.0\,\text{min}^{-1}$ and the temperatures indicated.

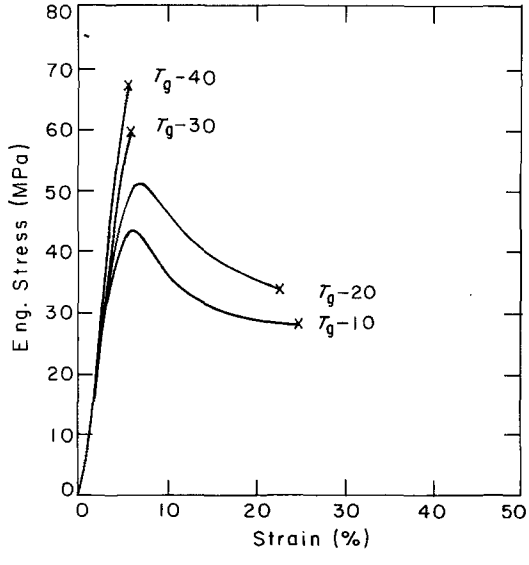

Figure 7 Engineering stress–strain curves for blend 10/90 at $\dot{\varepsilon} = 10.0\,\text{min}^{-1}$ and the temperatures indicated.

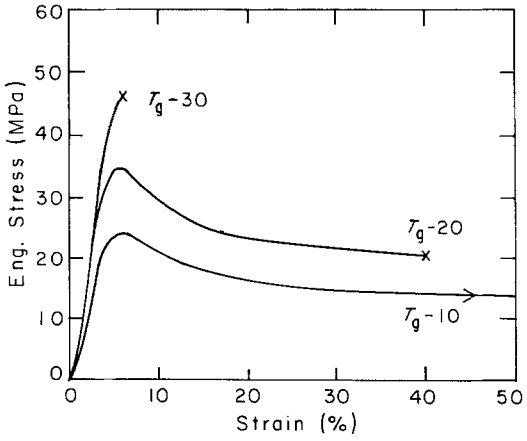

Figure 8 Engineering stress–strain curves for PMMA homopolymer at $\dot{\varepsilon} = 10.0\,\text{min}^{-1}$ and the temperatures indicated.

stresses lower than those seen in 10/90. Modulus and strain-to-break are also lower in 0/100 than in 10/90.

Fig. 10 shows the tensile behaviour of the blends at the highest relative test temperature at T_g-10. Two extreme strain rates are shown, $10.0\,\text{min}^{-1}$ (Fig. 10a) and $0.01\,\text{min}^{-1}$ (Fig. 10b). Homopolymer PVF_2 was not tested at $10.0\,\text{min}^{-1}$. In Fig. 10a, starting with 90/10, the trends seen in Fig. 9 carry over to the T_g-10 test conditions. Drawing stress and modulus decrease in the order 90/10 > 75/25 > 60/40 > 40/60. Breaking strains increase from 90/10 to 40/60, with the latter drawing to 148% before failure. Further increase in PMMA content in 10/90 again leads to a jump in tensile properties. Yield stress and modulus are higher, and breaking strain is lower, in 10/90 compared to 40/60. The PMMA homopolymer modulus, yield stress, and drawing stress beyond yield are lower than 10/90 continuing the trend seen in Fig. 9.

At the very slowest strain rate and highest test temperature, shown in Fig. 10b, the trends in drawing stress and strain-to-break are the same as previously described with but a few differences. Premature failure of 100/0 may be the reason for its fracture stress being lower than in 90/10. A very large difference in stress level can now be seen between 90/10 and 75/25. Both 60/40 and 40/60 drew to over 100% strain but testing was halted before failure occurred because of the time involved in testing at this slow strain rate. At the composition 10/90, the modulus and drawing stress once again increase compared to 40/60, and strain-to-break decreases. Homopolymer PMMA (0/100) drew at a very low, constant stress level to a breaking strain of 95%. In general, the yield and breaking stresses decrease, and breaking strains increase, as the strain rate decreases from 1.0 to $0.01\,\text{min}^{-1}$. All blends exhibit increased drawability, i.e. reduced drawing stresses and increased breaking strains, as the strain rate decreases from $10\,\text{min}^{-1}$ (Fig. 10a) to $0.01\,\text{min}^{-1}$ (Fig. 10b), or as the test temperature increases (Figs 9a, b).

Blends 60/40, 40/60 and 10/90 (Fig. 10b) could be drawn to very large breaking strains at nearly constant engineering stress. This behaviour is observed under drawing conditions of low strain rate and high drawing temperature which are known to favour chain disentanglement. In these blends, no intrinsic yield point is observed. That is, a plot of true stress against nominal strain did not exhibit strain softening but instead showed a steadily increasing stress level beyond the extrinsic yield point as determined from a Consideres construction.

3.3. Stress–strain behaviour: effects of composition

We explored further the effects of composition on the yield behaviour. In Figs 11a and b we show the true yield stress plotted against actual test temperature at all the strain rates. Amorphous blend 40/60 is shown

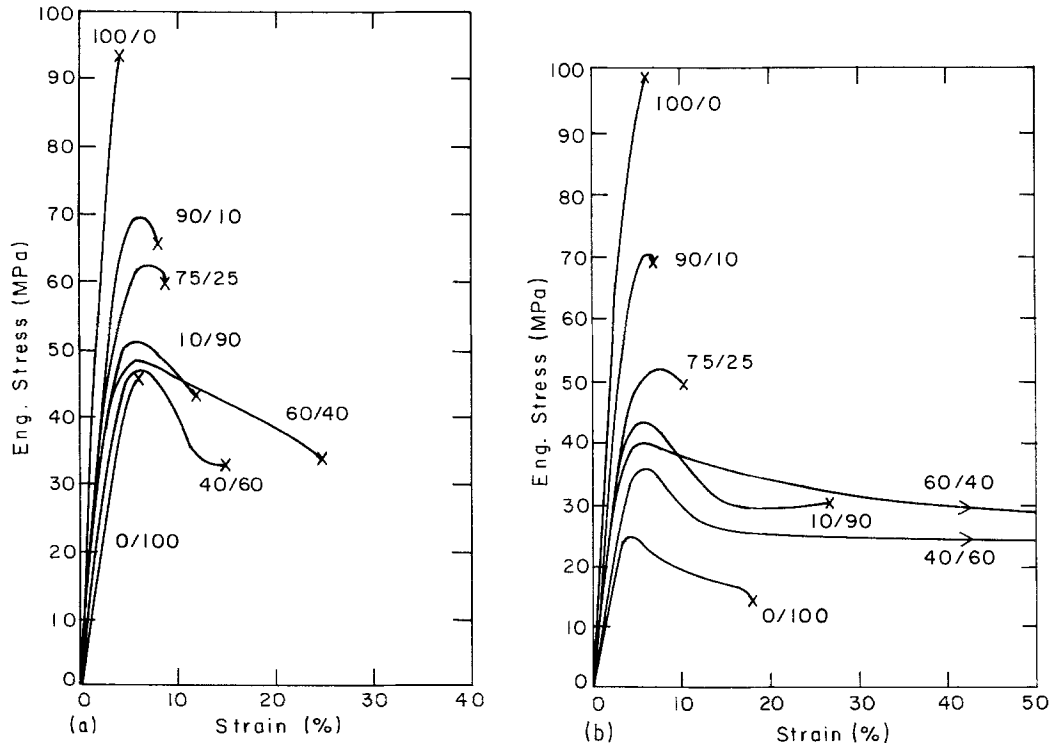

Figure 9 Engineering stress–strain curves for homopolymers and blends: (a) T_g-30, $1.0\,\text{min}^{-1}$; (b) T_g-20, $1.0\,\text{min}^{-1}$.

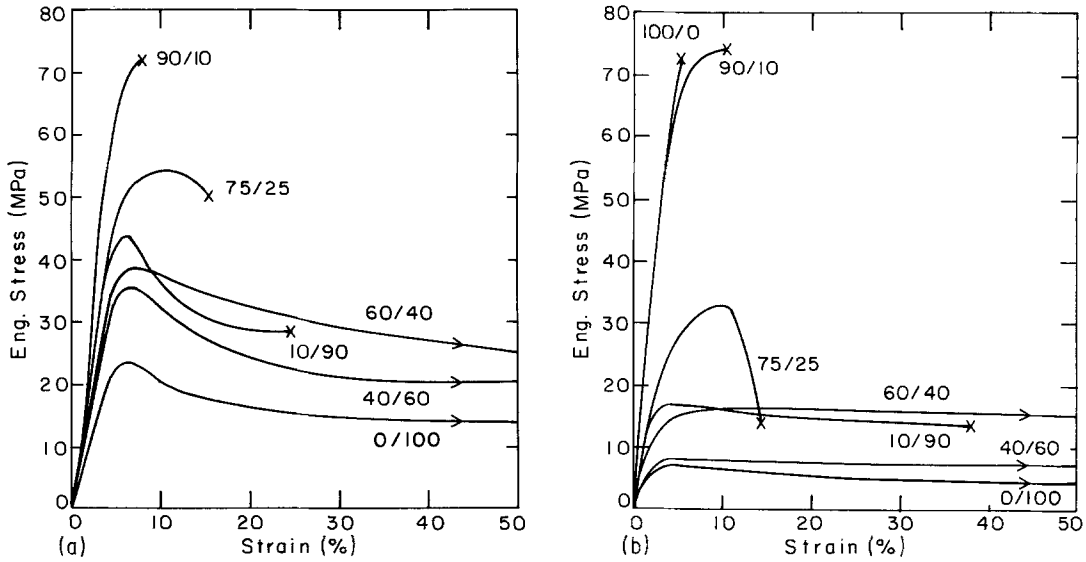

Figure 10 Engineering stress–strain curves for homopolymers and blends: (a) T_g-10, 10 min^{-1}; (b) T_g-10, 0.01 min^{-1}.

in Fig. 11a, and semicrystalline blend 75/25 in Fig. 11b. T_g is indicated by an arrow on the temperature axis. For each strain rate, the true yield stress decreases as the test temperature increases towards T_g. If a line were drawn through the data representing a fixed strain rate, the line would intersect the temperature axis when the yield stress drops to zero. For the amorphous blend 40/60 (and also for 10/90 which is not shown), the yield stress drops to zero for 0.01 min^{-1} at a temperature very close to the glass transition temperature, as shown by the dashed line. In contrast, the semicrystalline blends had generally much larger yield stresses. For 75/25 shown in Fig. 11b (and also for 60/40 which is not shown), the yield stress falls to zero, by extrapolation, at a temperature much higher than the glass transition temperature for the strain rates tested. This reinforcing effect of crystals in blend materials suggests that the blends may be able to undergo physical ageing at temperatures above their nominal glass transitions.

Three blends, 75/25, 60/40 and 40/60, were aged at 45° C for very long times, then tested in tension at room temperature, at a strain rate of 0.01 min^{-1}. In Fig. 12, these results are shown along with those for the unaged materials. Because the ageing temperature was fixed, while T_g varies with composition, here we have a situation in which 75/25 ages at a temperature above its T_g, 60/40 below its T_g, and 40/60 just at its T_g. For all the aged blends, modulus and drawing stress increased over the unaged materials. As in all other tests of unaged 75/25, the aged blend exhibits no sharp yield point. For 60/40 and 40/60, a distinct yield point is followed by drawing at constant stress. Tests of the latter two blends were halted prior to fracture.

4. Discussion

From Figs 9 and 10, and the data summarized in Tables II to IV, we can arrive at a general description of the stress–strain behaviour of these materials as a function of strain rate and normalized test temperature. Compared to the blends, homopolymer PVF_2 had the largest drawing stress under all test conditions. The PVF_2 stress–strain curves were not linear, as might be the case for strictly brittle fracture. The

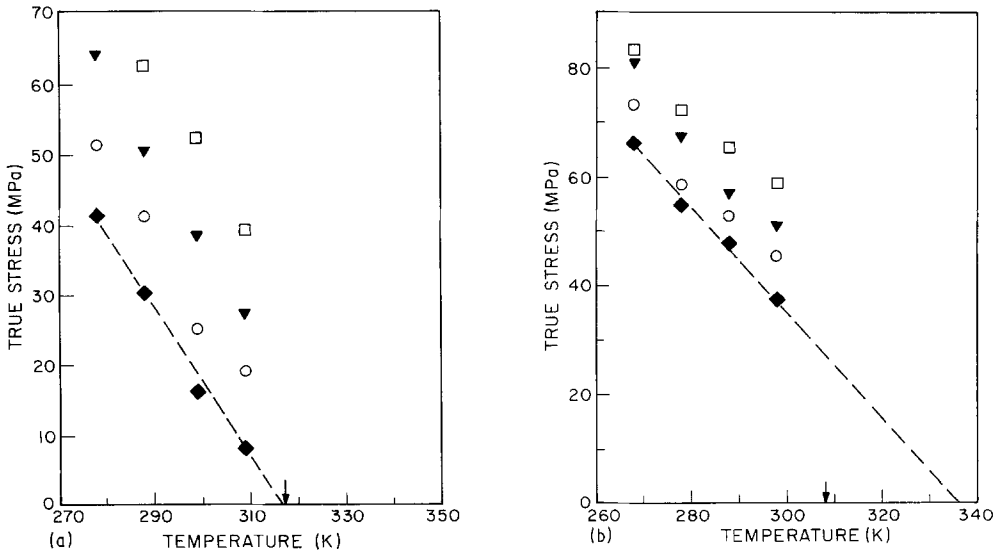

Figure 11 Variation of true yield stress with absolute drawing temperature, as a function of strain rate. The arrow marks the location of T_g. (a) Amorphous blend 40/60, (b) semicrystalline blend 75/25. (□) 10.0 min^{-1}, (▼) 1.0 min^{-1}, (○) 0.1 min^{-1}, (◆) 0.01 min^{-1}.

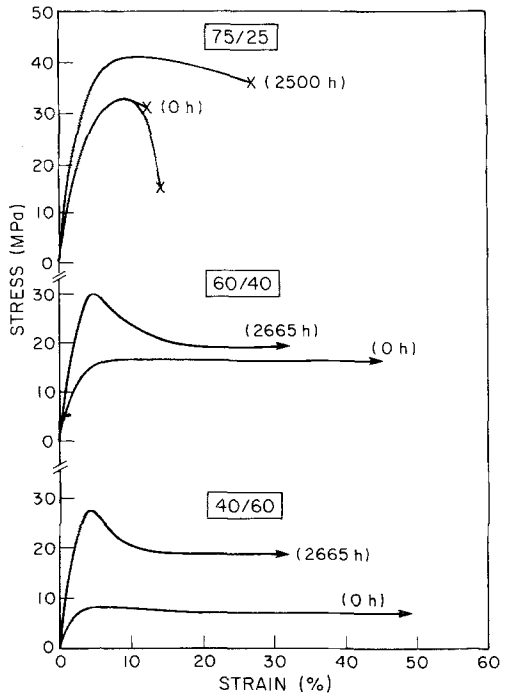

Figure 12 Engineering stress–strain curves for unaged (0 h) and aged blends. Blends were aged at 45° C for the times indicated, then tested at room temperature at 0.01 min^{-1}.

curves at higher strain levels showed a decrease in modulus from that seen in the low strain (under 1%) region. PVF_2 broke at strains of about 4% to 7% without showing any yield. With no PMMA chains in the amorphous regions, interlamellar tie molecules have the greatest effect in pure PVF_2 tensile behaviour, resulting in the highest moduli and breaking stresses.

In view of the very small difference in degree of crystallinity between 75/25 and 90/10 the large variation in tensile properties is remarkable. The change from very brittle-like failure in 90/10 to a more ductile deformation in 75/25 cannot reasonably be attributed to the very small decrease in crystallinity. On the assumption that yield behaviour is controlled by the amorphous regions, we may understand the differences between 90/10 and 75/25 if, instead of degree of crystallinity, we consider the PVF_2 composition of the amorphous phase. The ratio of amorphous PVF_2 to PMMA is much greater in 90/10 (a-PVF_2/PMMA = 82/18) than in 75/25 (a-PVF_2/PMMA = 57/43). The large variation in the yield behaviour of 90/10 compared to 75/25 is most likely due to the large ratio of amorphous PVF_2 to PMMA in the former.

In our PVF_2/PMMA samples 90/10 and 75/25, spherulites completely fill the available volume as they have been observed to do in other blend studies [16, 24]. From this, we know that the PMMA is not residing between spherulites, but rather between or alongside the PVF_2 lamellae. The PMMA is not uniformly mixed with the amorphous PVF_2, but is excluded from a region near the crystal surfaces by a boundary layer of PVF_2 [24, 25]. Hahn *et al.* [25] claim that the interphase of amorphous PVF_2 and the crystalline phase are in 1 : 1 proportion by weight. In our materials this cannot be the case. In blends 60/40 and 75/25, for example, the blends are of sufficiently high crystallinity that the assumption of a 1 : 1 proportion would essentially remove all PVF_2 chains from mixing with the PMMA. This is in conflict with our observation of a single glass transition, intermediate between the T_gs of PVF_2 and PMMA.

In Figs 13a and b, a schematic illustration of the

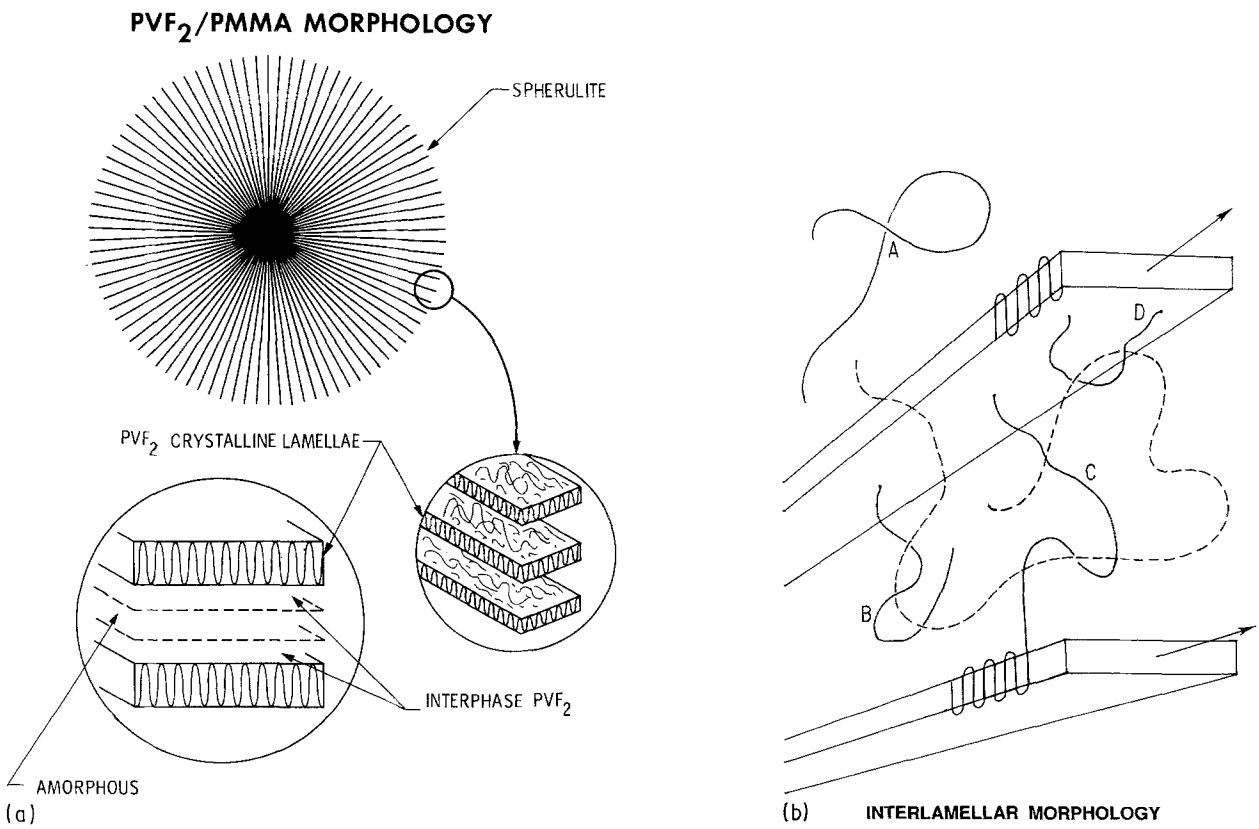

Figure 13 (a) Spherulite with expanded view of the interlamellar region. Pure PVF_2 occupies the interface nearest the lamellar surfaces. Amorphous PVF_2 and PMMA mix freely far from the lamellae. (b) Schematic illustration of interlamellar morphology of semicrystalline blends. (– – –) PMMA chain; (——) PVF_2 chains with varying degrees of interlamellar connection.

interlamellar morphology of the semicrystalline blends is depicted. In Fig. 13a the spherulite morphology is shown, with an expanded view of the interlamellar region. Next to the crystal surfaces is an interphase region with pure PVF_2 [24, 25], and further away is a layer consisting of mixed amorphous PVF_2 and PMMA. A very simplified sketch is shown in Fig. 13b depicting four PVF_2 chains (solid lines) surrounding a PMMA chain (dashed line). Two adjacent lamellae are shown growing outward in the direction of the arrows from the same spherulite centre (not shown). PVF_2 chain A is completely free of any crystallite entanglement. It can mix freely with the PMMA chains, and is the only type of PVF_2 chain found in the completely amorphous blends 40/60 and 10/90. PVF_2 chains B, C and D represent varying levels of crystalline entanglement. Chain B has one end emerging from the fold surface, while the other end is free. Chains C and D have both chain ends embedded in lamellae, but chain C connects two different lamellae while D is entangled at both ends in the same lamella. Depending on the thickness of the interphase layer, a loose loop, like chain D, may entangle with the PMMA as depicted. However, it has been suggested that re-entry of a PVF_2 chain into the same lamella may occur only in the region where PMMA is excluded [25]. Chains like B and C provide physical entanglement to the PMMA chains. While the PMMA chains are excluded from the interphase region near the crystal surfaces [24, 25], they nonetheless can feel the reinforcing effects of the crystals through PVF_2 chains B and C. Chains like B and C are responsible for the very large differences in tensile behaviour seen in the semicrystalline blends. The higher the proportion of amorphous PVF_2 to PMMA, the greater the number of chains of types B and C which will surround and entangle the remaining PMMA.

For blends with about the same degree of crystallinity, like 90/10 and 75/25, the decrease in the ratio of a-PVF_2/PMMA for 75/25 means that the PMMA may make interlamellar ties (PVF_2 chains C) less likely to form. First, there is a smaller amount of PVF_2 available for inclusion in the amorphous phase after crystallization is completed. Second, the PMMA may intervene such as to prevent, or at least reduce, interlamellar connections. Reduction of interlamellar entanglements could explain the very large differences in the tensile behaviour between 90/10 and 75/25. Under conditions favouring disentanglement, i.e. high relative test temperature and slow strain rate (Fig. 10b), the largest differences in tensile behaviour are seen for 90/10 compared to 75/25.

Another pair of blends provides further support for the idea that the crystals act to anchor PVF_2 chains. Blend 60/40 can be compared to 40/60: these two materials have nearly the same relative proportions of a-PVF_2 and PMMA. In 60/40 a-PVF_2/PMMA = 37/63 and in 40/60 the ratio is a-PVF_2/PMMA = 40/60. The difference is that 60/40 is semicrystalline with a degree of crystallinity of 37%. The amorphous PVF_2 chains B and C in 60/40 will be tied to the crystalline phase, whereas in 40/ 60 the amorphous PVF_2 chains A are unconstrained.

In all testing situations, the general behaviour of 60/40 is very similar to 40/60, and always dissimilar compared to 75/25. The drawability of 60/40 and 40/60, as indicated by the shape of the stress–strain curves in Figs 9 and 10, is similar. The main difference is that larger stress level is required to draw 60/40 to the same strain level. The large amount of PMMA intervening between the crystals in 60/40 may affect the drawing behaviour through a reduction in initial formation of interlamellar entanglement chains of PVF_2 type C. If, on the other hand, very strong interlamellar ties were formed in 60/40, we might except a decrease in the strain-to-break at test conditions of low temperature and high strain rate. In fact the opposite is seen, the breaking strains in 60/40 being sometimes quite a bit larger than 40/60 under conditions unfavourable to disentanglement. This suggests that interlamellar ties are not the controlling feature in the tensile drawing of 60/40. The lamellar crystals seem to be acting as isolated reinforcement causing the drawing stresses to be greater than in 40/60, but having little effect on breaking strain.

The relationships among the completely amorphous materials are more difficult to interpret, though a regular pattern exists in the stress–strain curves. Consider first the pure PMMA as compared to blend 10/90. Addition of a small amount of PVF_2 chains of type A results in a 10° C decrease in the glass transition temperature, and a large increase in modulus, yield stress and drawing stress in 10/90. Here the meaning of a "small amount" may be related to the interaction of PVF_2 chains solely with PMMA chains; it is unlikely that PVF_2 chains will be able to interact with other PVF_2 chains at this composition. Evidence for isolation of the PVF_2 chains in 10/90 may also be deduced from the inability of the blend to crystallize for low PVF_2 content [3, 19, 30, 33].

An increase from 10 to 40 wt % PVF_2 results not only in further reduction of the glass transition, but also in a decrease in modulus, yield stress, and drawing stress. At 40 wt %, the PVF_2 chains will interact with neighbouring PVF_2 as well as with the PMMA. Blends with this composition ratio have been crystallized under conditions of long annealing [51], an indication that proximity of PVF_2 chains of type A occurs in this composition. This interaction may be responsible for the increased drawability of 40/60. Our limited data on two amorphous blend compositions support this interpretation, but in order to explore fully the effects of PFV_2 type A chains, further investigations must be undertaken with smaller incremental changes in the PVF_2 composition.

In reviewing other work in tensile properties of PVF_2/PMMA blends [1, 35, 36], we have found it very difficult to make detailed comparisons because there is no overlap of testing conditions and starting materials. Therefore we consider it most reasonable to compare on the basis of general trends, and not on the specifics of yield stress, fracture stress, etc. Ullman and Wendorff [35] performed most of their tests above T_g though the increment above T_g varied for each blend. Our work may be considered complementary in the sense that all our testing is done at fixed increments

below T_g. The general trends of yield stress decreasing with increase in test temperature in amorphous blends ([35], Fig. 6) agree well with the composition variation shown here in Fig. 11 and Table II. We tested both amorphous and semicrystalline blends, and find that in the former, yield stress decreases rapidly as test temperature approaches T_g. In the semicrystalline blends, interlamellar entanglements result in values of yield stress which remain very high, and appear to extrapolate to zero yield stress at temperatures well above T_g.

Woan's work [36] reports the composition dependence of tensile properties for blends tested at fixed temperatures. The main conclusion of Woan's work was observation of brittle–ductile transitions between 30/70 and 40/60 when testing at 25° C, 0.25 cm min^{-1} (see Fig. 87 of [36]). Both of the blends in Woan's case were studied below T_g. Blend 30/70 was tested at about T_g-65, and 40/60 was tested at T_g-50,using normalized test temperature and T_gs obtained from [36], Fig. 11. In our case, a composition dependence of the brittle-ductile transition may be of greater significance because all blends are tested at the same relative temperature. We find the brittle–ductile transition occurs between 90/10 (brittle) and 75/25 (ductile) for nearly all testing conditions. Only at T_g-40 at fast rates (10.0 and 1.0 min^{-1}) was 75/25 brittle.

Our observation of physical ageing in semicrystalline blends, both below and above the single glass transition, can be interpreted using the model put forth by Struik [52, 53]. In Struik's model, ageing takes place between T_g and T_β, the temperature of the highest secondary relaxation, in purely amorphous materials. But for the semicrystalline materials, physical ageing may occur above T_g. Struik attributes the latter to the existence of chain constraints which result in the broadening of the glass transition.

In the blends, we envisage a region far from the crystals where PVF_2 and PMMA are miscible and, above T_g, fluid-like. Closer to the crystals, PVF_2 chains become less flexible due to entanglement with the crystals. In the case of no intervening PMMA, all the PVF_2 may be constrained, as suggested by the dielectric studies of Hahn *et al.* [24]. It seems reasonable to explain the physical ageing of the semicrystalline blends in an analogous manner to homopolymers using Struik's model. When aged blends were subsequently scanned in a DSC, they exhibited a single glass transition and the ageing peak [51] as described earlier.

5. Conclusions

The tensile properties of PVF_2/PMMA blends have been measured at a variety of strain rates for test temperatures normalized to fixed increments below T_g. Thus all blends are tested under conditions designed to minimize the effects of absolute test temperature. Summarizing our results, we find that nearly all blends drew to increased breaking strains, as the strain rate became slower or as test temperature approached T_g. Materials 100/0 and 90/10 were brittle-like, and their behaviour was more erratic.

For materials with about the same degree of crystallinity (100/0, 90/10, 75/ 25), the content of the amorphous regions may play a key role in tensile behaviour. Reduction of interlamellar PVF_2 tie molecules may occur as PMMA content increases, resulting in increased drawability. Where interlamellar ties would be weakest, in 60/40, the tensile behaviour was very similar to that of amorphous 40/60. Both amorphous and semicrystalline blends experienced physical ageing, but the latter could be aged above T_g, providing further evidence of the importance of interlamellar ties.

Acknowledgements

This work was performed at the Jet Propulsion Laboratory, California Institute of Technology, under contract with the National Aeronautics and Space Administration.

References

1. J. S. NOLAND, N. N.-C. HSU, R. SAXON and J. M. SCHMITT, *Adv. Chem. Ser.* **99** (1971) 15.
2. E. ROERDINK and G. CHALLA, *Polymer* **19** (1978) 173.
3. D. R. PAUL and J. O. ALTAMIRANO, *Adv. Chem. Ser.* **142** (1975) 371.
4. D. J. HOURSTON and I. D. HUGHES, *Polymer* **18** (1977) 1175.
5. G. D. PATTERSON, T. NISHI and T. T. WANG, *Macromol.* **9** (1976) 603.
6. G. DIPAOLA-BARANYI, S. J. FLETCHER and P. DEGRE, *ibid.* **15** (1982) 885.
7. D. C. DOUGLASS and J. V. McBRIERTY, *ibid.* **11** (1978) 766.
8. T. C. WARD and T. S. LIN, *Adv. Chem. Ser.* **206** (1984) 59.
9. P. TEKELY, F. LAUPRETRE and L. MONNERIE, *Polymer* **26** (1985) 1801.
10. M. M. COLEMAN, J. ZARIAN, D. F. VARNELL and P. C. PAINTER, *J. Polym. Sci. Polym. Lett. Edn.* **15** (1977) 745.
11. R. E. BERNSTEIN, C. A. CRUZ, D. R. PAUL and J. W. BARLOW, *Macromol.* **10** (1977) 681.
12. Y. HIRATA and T. KOTAKA, *Polym. J.* **13** (1981) 273.
13. T. T. WANG and T. NISHI, *Macromol.* **10** (1977) 421.
14. W. H. JO and D. H. BAIK, *Polymer (Korea)* **8** (1984) 204.
15. B. MORRA and R. S. STEIN, *J. Polym. Sci. Polym. Phys. Edn.* **20** (1982) 2243.
16. *Idem, ibid.* **20** (1982) 2261.
17. *Idem, Polym. Engng Sci.* **24** (1984) 311.
18. C. LEONARD, J. HALARY and L. MONNERIE, *Macromol.* **21** (1988) 2988.
19. T. NISHI and T. T. WANG, *ibid.* **8** (1975) 909.
20. J. PLANS, W. J. MACKNIGHT and F. E. KARASZ, *ibid.* **17** (1984) 1100.
21. J. RUNT and P. B. RIM, *Proc. ACS Div. Polym. Mater. Sci.* **51** (1984) 295.
22. H. SAITO, Y. FUJITA and T. INOUE, *Polym. J.* **19** (1987) 405.
23. S. SHIMADA, Y. HORI and H. KASHIWABARA, *Macromol.* **21** (1988) 3454.
24. B. HAHN, J. WENDORFF and D. Y. YOON, *ibid.* **18** (1985) 718.
25. B. R. HAHN, O. HERMANN-SCHONHERR and J. H. WENDORFF, *Polymer* **28** (1987) 201.
26. J. S. CHIOU and D. R. PAUL, *Polym. Engng Sci.* **26** (1986) 1218.
27. H.-K. CHUANG and C. D. HAN, *J. Appl. Polym. Sci.* **29** (1984) 2205.
28. C. DOMENICI, D. DE ROSSI, A. NANNINI and R. VERNI, *Ferroelect.* **60** (1984) 61.
29. G. K. N. RASHMI and P. K. C. PILLAI, *J. Macro. Sci. Phys.* **B26** (1987) 185.

30. B. SERVET, D. BROUSSOUX, S. RIES and F. MICHERON, *Mater. Sci. Monographs* **21** (1984) 81.
31. J. K. KRUGER, A. MARX, R. ROBERTS, H.-G. UNRUH and J. H. WENDORFF, *Ferroelect.* **55** (1984) 147.
32. B. R. HAHN and J. H. WENDORFF, *Polymer* **26** (1985) 1619.
33. D. R. PAUL and J. O. ALTAMIRANO, *Polym. Preprint* **15** (1974) 409.
34. B. SERVET, D. BROUSSOUX and F. MICHERON, *J. Appl. Phys.* **52** (1981) 5926.
35. W. ULLMANN and J. H. WENDORFF, *Comp. Sci. Tech.* **23** (1985) 97.
36. D.-J. WOAN, PhD thesis, Rutgers State University of New Jersey, (1984).
37. K. NAKAGAWA and Y. ISHIDA, *J. Polym. Sci. Polym. Phys. Edn* **11** (1973) 2153.
38. S. OSAKI and Y. ISHIDA, *ibid.* **13** (1975) 1071.
39. W. M. PREST and D. J. LUCA, *J. Appl. Phys.* **49** (1978) 5042.
40. M. J. RICHARDSON and N. G. SAVILL, *Brit. Polym. J.* **11** (1979) 123.
41. J. B. LANDO and W. W. DOLL, *J. Macromol. Sci. Phys.* **B2** (1968) 205.
42. S. WEINHOLD, M. H. LITT and J. B. LANDO, *J. Polym. Sci. Polym. Lett. Edn* **17** (1979) 585.
43. R. HASEGAWA, Y. TAKAHASHI, Y. CHATANI and H. TADOKORO, *Polym. J.* **3** (1972) 600.
44. C. LEONARD, J. HALARY, L. MONNERIE, D. BROUSSOUX, B. SERVET and F. MICHERON, *Polym. Commun.* **24** (1983) 110.
45. M. KOBAYASHI, K. TASHIRO and H. TADOKORO, *Macromol.* **8** (1975) 158.
46. M. A. BACHMANN, W. L. GORDON, J. L. KOENIG and J. B. LANDO, *J. Appl. Phys.* **50** (1979) 6106.
47. R. HASEGAWA, M. KOBAYASHI and H. TADOKORO, *Polym. J.* **3** (1972) 591.
48. D. T. GRUBB and K. W. CHOI, *J. Appl. Phys.* **52** (1981) 5908.
49. D. T. GRUBB, P. CEBE and K. W. CHOI, *Ferroelect.* **57** (1984) 121.
50. P. B. BOWDEN, in "The Physics of Glassy Polymers", edited by R. N. Haward (Applied Science, London, 1973) Ch. 5, p. 279.
51. P. CEBE and S. Y. CHUNG, unpublished results (1986).
52. L. C. E. STRUIK, *Polymer* **28** (1987) 1521.
53. *Idem, ibid.* **28** (1987) 1534.

Received 21 February
and accepted 24 August 1989